International Journal of Pharmaceutics 644 (2023) 123333

Contents lists available at ScienceDirect

International Journal of Pharmaceutics

journal homepage: www.elsevier.com/locate/ijpharm

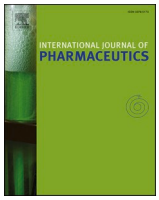

Amorphous solid dispersions of curcumin in a poly(ester amide): Antiplasticizing effect on the glass transition and macromolecular relaxation dynamics, and controlled release

Sofia Valenti [a,b,c], Matteo Arioli [b], Alex Jamett [c], Josep Lluís Tamarit [a,c], Jordi Puiggalí [a,b,d], Roberto Macovez [a,c,*]

[a] Barcelona Research Center in Multiscale Science and Engineering, Universitat Politècnica de Catalunya, Campus Diagonal-Besòs, Av. Eduard Maristany 10-14, E-08019 Barcelona, Catalonia, Spain
[b] Synthetic Polymers: Structure and Properties. Biodegradable Polymers, Departament de Enginyeria Química, Universitat Politècnica de Catalunya, EEBE, Av. Eduard Maristany 10-14, E-08019 Barcelona, Catalonia, Spain
[c] Grup de Caracterització de Materials, Departament de Física, Universitat Politècnica de Catalunya, EEBE, Av. Eduard Maristany 10-14, E-08019 Barcelona, Catalonia, Spain
[d] Institute for Bioengineering of Catalonia (IBEC), The Barcelona Institute of Science and Technology (BIST), Carrer Baldiri i Reixac 11-15, E-08028 Barcelona, Catalonia, Spain

ARTICLE INFO

Keywords:
Amorphous formulations
Glass transition temperature
Kinetic stability
Molecular mobility
Dielectric spectroscopy
Release kinetics

ABSTRACT

In order to exploit the pharmacological potential of natural bioactive molecules with low water solubility, such as curcumin, it is necessary to develop formulations, such as amorphous polymer dispersions, which allow a constant release rate and at the same time avoid possible toxicity effects of the crystalline form of the molecule under scrutiny. In this study, polymer dispersions of curcumin were obtained in PADAS, a biodegradable semicrystalline copolymer based on 1,12-dodecanediol, sebacic acid and alanine. The dispersions were fully characterized by means of differential scanning calorimetry and broadband dielectric spectroscopy, and the drug release profile was measured in a simulated body fluid. Amorphous homogeneous binary dispersions were obtained for curcumin mass fraction between 30 and 50%. Curcumin has significantly higher glass transition temperature T_g (≈ 347 K) than the polymer matrix (≈274-277 K depending on the molecular weight), and dispersions displayed T_g's intermediate between those of the pure amorphous components, implying that curcumin acts as an effective antiplasticizer for PADAS. Dielectric spectroscopy was employed to assess the relaxation dynamics of the binary dispersion with 30 wt% curcumin, as well as that of each (amorphous) component separately. The binary dispersion was characterized by a single structural relaxation, a single Johari-Goldstein process, and two local intramolecular processes, one for each component. Interestingly, the latter processes scaled with the T_g of the sample, indicating that they are viscosity-sensitive. In addition, both the pristine polymer and the dispersion exhibited an interfacial Maxwell-Wagner relaxation, likely due to spatial heterogeneities associated with phase disproportionation in this polymer. The release of curcumin from the dispersion in a simulated body fluid followed a Fickian diffusion profile, and 51% of the initial curcumin content was released in 48 h.

1. Introduction

Biocompatible polymers are widely used to tune drug release and enable drug delivery applications. On one hand, dispersion of poorly-soluble drugs in water-soluble amorphous biopolymers (Romanini et al., 2018) improves the dissolution kinetics and drug concentration in aqueous media (Szczurek et al., 2017). On the other hand, water-insoluble biodegradable polymers can be used as carriers for slow, controlled release of drugs that must be administered over prolonged periods of time and to create scaffolds for tissue growth (Liechty et al., 2010), with the advantage that the carrier or scaffold are biodegraded and metabolized without need of removal.

* Corresponding author.
E-mail address: roberto.macovez@upc.edu (R. Macovez).

https://doi.org/10.1016/j.ijpharm.2023.123333
Received 24 February 2023; Received in revised form 20 July 2023; Accepted 17 August 2023
Available online 18 August 2023

Among biodegradable polymers, poly(ester amide)s are considered promising materials for biomedical applications as they combine the biodegradable character of the hydrolizable ester groups with the relatively good thermal stability and mechanical properties conferred by intermolecular hydrogen bonding mediated by the amide groups, thereby merging the beneficial properties of polyesters and polyamides into a single copolymer (Rodriguez-Galan et al., 2011; Fonseca et al., 2014; Winnacker and Rieger, 2016; Han and Wu, 2022). Despite their application potential, the dynamic macromolecular properties of these polymers have not been probed by spectroscopic techniques specialized for amorphous and semicrystalline polymers such as broadband dielectric spectroscopy.

In this contribution we investigate the molecular relaxation dynamics of a home-synthesized poly(ester amide)s based on 1,12-dodecanediol, sebacic acid, and alanine in two distinct chiral forms (Paredes et al., 1998), as well as of amorphous curcumin dispersions in these polymers. Curcumin has high anti-oxidant and antimicrobial power (Srinivasan, 2014; Ak and Gülçin, 2008; De et al., 2009), and has recently attracted the interest of the research community for its anti-inflammatory and especially anti-carcinogenic properties (Priyadarsini, 2014; Aggarwal et al., 2013; Dhillon et al., 2008; Bar-Sela et al., 2010; Sanphui and Bolla, 2018). This bioactive compound has extremely low solubility in water and poor intestinal absorption, which hinder its bioavailability (Yang et al., 2013; Pawar et al., 2012; Aggarwal and Sung, 2009; Anand et al., 2007), and controlled drug release strategies may represent a way to improve its effectiveness. The polymer chosen for the dispersions displays a tunable enzymatic degradation rate (Rodríguez-Galán et al., 1999), is not cytotoxic (Paredes et al., 1998), and has been already employed to fabricate a microsphere matrix for drug delivery systems (Rodriguez-Galan et al., 2011) and as the main constituent of electrospun scaffolds with either an anti-microbial (chlorohexidine) or an anti-inflammatory (ibuprofen) agent (del Valle et al., 2011, Del Valle et al. (2012)).

The goal of this work is both to unravel macromolecular mobility of poly(ester amide)s, and to achieve stable dispersions of curcumin in a biodegradable polymer matrix with mechanical properties that allow the fabrication of sutures and other drug delivery systems. Scanning calorimetry and dielectric spectroscopy are employed to analyze the thermodynamic and molecular relaxation dynamic properties of pure amorphous curcumin, of the pure poly(ester amide) samples, and of curcumin amorphous polymer dispersions. The focus is both on primary (structural) and secondary relaxations, the former as they are directly responsible for the glass transition properties of the resulting dispersions, and the latter because understanding the kinetic stability of the glass requires a knowledge of secondary relaxation processes taking place in it (Zhou et al., 2002; Gupta et al, 2004; Bhardwaj et al., 2013; Kissi et al., 2018).

In this contribution, the polymer is shown to display a very rich relaxation behavior, which includes a structural (segmental) relaxation associated with the glass transition temperature, T_g, a Maxwell-Wagner relaxation typical of copolymers, a Johari-Goldstein relaxation, and an intra-chain relaxation likely associated with the conformational changes of the ester groups. The amorphous binary dispersion has even richer relaxation behavior. It is shown that curcumin, having higher T_g than the polymer, has an antiplasticizing effect on it, with the T_g of binary amorphous dispersions increasing linearly with curcumin weight content. As expected, the structural relaxation time increases with curcumin content. The secondary losses, which as mentioned may facilitate crystallization of the amorphous dispersions below T_g, are also analyzed. Finally, the release of curcumin from a 30% amorphous solid dispersion in PADAS is studied using a simulated body fluid. It is found that after 48 h already half the drug is released, which is a significantly higher percentage than the typical values obtained with simple polyesters (Valenti et al., 2019).

2. Materials

2.1. Synthesis of poly(ester amide)

The poly(ester amide) was synthesized following a polymerization strategy detailed in previous studies (Paredes et al., 1998). For this purpose, L- and D-alanine, 1,12-dodecanediol, sebacic acid, carbon tetrachloride and sodium carbonate were purchased from Sigma Aldrich, and p-toluene sulfonic acid monohydrate was purchased from Alpha Aesar. All reagents were ACS grade and used without previous purification.

Briefly, the p-toluensulfonic salt of bis-(alanine) 1,12-dodecamethylene diestearate was first synthesized. This compound was used as a monomer unit to react with the sebacoyl dichloride monomer, via interfacial polycondensation using carbon tetrachloride as organic solvent and sodium carbonate as proton acceptor. A solution of the monomer (0.003 mol) and the proton acceptor (0.006 mol of Na_2CO_3) in a mixture of water (34 mL) and acetone (2 mL) was added to 22 mL of a solution of the dichloride (0.003 mol) in CCl_4. A brittle film immediately appeared in the interphase. After stirring for 30 min at high speed, the polymer was filtered and repeatedly washed with CCl_4, water, ethanol, and ether, before drying in a vacuum desiccator at 333 K. The resulting polymer, which can be described by the sequence poly(alanine-dodecanediol-alanine-sebacic acid), is hereafter referred to as PADAS. Either L-alanine were used, to obtain enantiomeric pure L-PADAS, or a 50:50 mixture of D and L enantiomers of alanine, yielding the racemic D, L-PADAS. The latter polymer was synthesized with the aim of obtaining a larger amorphous fraction (all synthetized polymers were semicrystalline).

2.2. Preparation of curcumin dispersions

Curcumin ($C_{21}H_{20}O_6$, $M_w = 368.38$ g mol^{-1}) with purity better than 98% was purchased from Sigma-Aldrich and used as received. In order to obtain dispersion of curcumin in PADAS, the polymer was dissolved in chloroform at 10 % (w/v) concentration during one day. A dissolution of curcumin in ethanol (1%-w/v) was then added to obtain the desired PADAS-curcumin w/w ratio. The resulting solution was then solvent cast to a petri dish and a very brittle film was recovered after one day of drying.

3. Experimental methods

3.1. Verification of polymer synthesis

The chemical composition of the polymer was ascertained by Fourier-transform infrared spectroscopy and by NMR spectroscopy. GPC was used to assess molecular weight and polydispersity index (PDI) which were $M_w = 28363$ g mol^{-1} and PDI = 2.69 for L-PADAS and $M_w = 12380$ g mol^{-1} and PDI = 3.28 for D,L-PADAS.

3.2. Differential scanning calorimetry characterization

Differential scanning calorimetry (DSC) experiments were carried inside aluminum pans, by means of a Q100 from TA Instruments working in controlled nitrogen atmosphere with a flow rate of 25 mL min^{-1}. Heat-cool cycles were performed with a heating/cooling rate of 10 K min^{-1} and sample masses of about 5 mg (a microbalance sensitive to 0.01 mg was employed for mass determinations). Details of the temperature and enthalpy calibration of the device have been given elsewhere (Barrio et al., 2009). Temperature cycles were between 223 K and slightly above the melting point of the stable polymorph of curcumin ($T_m = 459$ K).

3.3. Dielectric spectroscopy characterization

For dielectric spectroscopy measurements, the samples were placed in a stainless steel parallel-plate capacitor specifically designed for the characterization of liquid samples. Temperature control of the capacitor was achieved with a nitrogen-gas flow cryostat (Novocontrol Quatro cryosystem) with an accuracy of 0.1 K. In the case of the pure materials, the curcumin powder and the dry polymer powder, these were melted directly inside the capacitor, while for the binary dispersions, the sample was first solvent cast upon the capacitor plates. In all cases, silica spacers of 50 μm diameter were employed to keep the two electrodes at fixed distance when the sample was in the melted state. In the case of polymer samples (pure PADAS as well as the binary dispersions), the melt inside the capacitor was rapidly cooled in order to obtain the most amorphous polymer possible, by inserting the capacitor in a cryostat held previously cooled down to the temperature of 123 K.

Isothermal complex relative permittivity spectra were acquired with a Novocontrol Alpha analyzer by increasing the temperature in a stepwise fashion. Spectra were recorded in the frequency range between 10^{-2} and 10^{6} Hz. To obtain relaxation times and quantify the changes in relaxation dynamics, the dielectric loss spectra (imaginary part of the complex permittivity spectra) were fitted as the sum of several model functions, one for each relaxation component, on top of a dc conductivity contribution of the form $-i\left(\frac{\sigma_0}{\varepsilon_0\omega}\right)^n$, where $\omega = 2\pi\nu$ is the angular frequency and n is an exponent close to unity. The model function was the imaginary part a Havriliak-Negami function, whose analytical expression is (Havriliak and Negami, 1967):

$$\varepsilon^*(\omega) = \varepsilon_\infty + \frac{\Delta\varepsilon}{(1+(i\omega\tau_0)^a)^b} \quad (1)$$

here, ε_∞ is the permittivity in the high frequency limit, $\Delta\varepsilon$ is the dielectric intensity or strength of the given relaxation process, the exponents a and b are shape parameters lying between 0 and 1, and τ_0 is a fit parameter. The characteristic relaxation time τ, corresponding to the maximum of the relaxation time distribution, is given in terms of the fit parameters as:

$$\tau = \tau_0\left[\sin\left(\frac{a\pi}{2b+2}\right)\right]^{-1/a}\left[\sin\left(\frac{ab\pi}{2b+2}\right)\right]^{1/a} \quad (2)$$

For data acquisition and fitting the WinData and WinFit programs were employed, provided for this purpose by the manufacturer (Novocontrol). The exponents a and b were let free to vary in the fit. This procedure showed that the so-called primary α relaxation, associated with the glass transition had an asymmetric line shape that could be well described by a Havriliak-Negami function with both a and b different from unity. Instead, all other relaxations, including secondary ones active in the glass state, had a symmetric profile, best described by a Cole-Cole function (Cole and Cole, 1942), a special case of Eq. (1) with $b = 1$, in which case the relaxation time reduces simply to τ_0.

To better visualize ac losses, the logarithmic derivative of the real part of the permittivity can be employed, defined as (Wübbenhorst and van Turnhout, 2002):

$$\varepsilon''_{der} = -\frac{\pi}{2}\frac{\partial\varepsilon'(\omega)}{\partial\ln(\omega)} \quad (3)$$

where $\varepsilon'(\omega)$ is the real part of the permittivity. The logarithmic derivative $\varepsilon''_{der}(\omega)$ is a good approximation to the dielectric loss $\varepsilon''(\omega)$ without the ohmic-conduction contribution. In all figures representing data obtained by means of dielectric spectroscopy, the associated experimental uncertainty is smaller than the marker size.

4. Results and discussion

4.1. Pure amorphous curcumin

Fig. 1 shows the calorimetric heat-cool-heat traces of curcumin. The possible tautomeric forms of curcumin in the liquid phase are shown in the inset. Polycrystalline curcumin is observed to melt at $T_m = 444$ K (peak), with an onset at significantly lower temperature, and no other melting peak is observed at higher temperature. The melting point of the stable crystalline form of curcumin, a monoclinic structure, is reported by previous studies to be 454.5 K; however, curcumin displays polymorphism, with three known crystalline structures, of which both metastable forms are orthorhombic (Sanphui et al., 2011; Thorat and Dalvi, 2015). The calorimetric melting onset of Fig. 1 might therefore correspond to the melting of a metastable orthorhombic phase, which is close enough to the melting of the stable monoclinic phase so that no recrystallization into the latter takes place in between 444 and 454 K. The molecule has twisted conformation in the monoclinic crystal, while it is linear and planar in both orthorhombic metastable crystal structures. It is likely that cross-conjugation contributes to the planar conformation of the molecular "arms", each constituted by a *o*-methoxyphenyl ring covalently linked with an ethylene moiety. These molecular "arms" are planar in both orthorhombic metastable forms, while one arm out of two is planar in the monoclinic stable structure.

Upon cooling from the liquid phase, the compound could be supercooled to the glass state, as visible in the second heat-up scan, which displays the typical specific-heat discontinuity associated with the glass transition at $T_g = 336 \pm 1$ K (onset), slightly lower (by 3 or 4 K) than reported in previous studies (Pawar et al., 2012; Minecka et al., 2019). Dielectric spectroscopy was employed to study the relaxation dynamics in curcumin. Compared with a previous study on the same compound (Minecka et al., 2019), we restrict ourselves to ambient pressure, but extend the experimental temperature range to lower values. As it will be shown, this allows us to identify a fast intramolecular relaxation of curcumin at low T. Fig. 2 shows selected isothermal loss spectra of curcumin in the amorphous state, namely both in the glass state below T_g and in the supercooled liquid state above T_g. Several loss components can be detected in these series of spectra, visible either as local maxima (structural relaxation) or as shoulders to the high-frequency side of the maximum (secondary relaxations). In order to extract characteristic relaxation times and shape parameters of the loss processes, all spectra

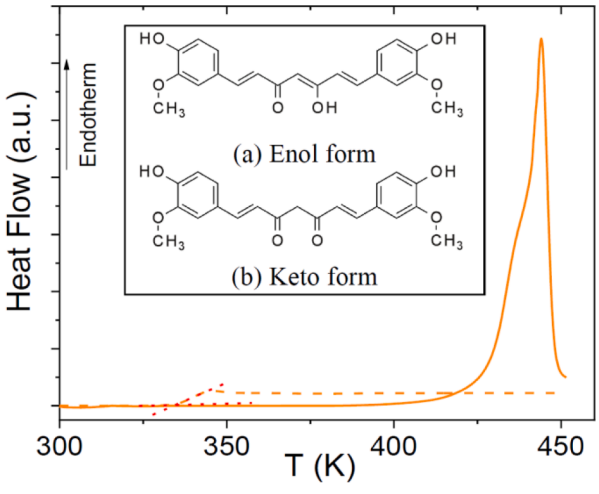

Fig. 1. First (continuous line) and second (dashed line) heat-up DSC traces of pure curcumin, measured upon heating the polycrystalline powder, then cooling from the liquid state into the glass state, and subsequently heating the resulting amorphous solid sample. The determination of the glass transition temperature is indicated by dotted lines. Insets: molecular structures of the two possible conformers of curcumin in the liquid phase.

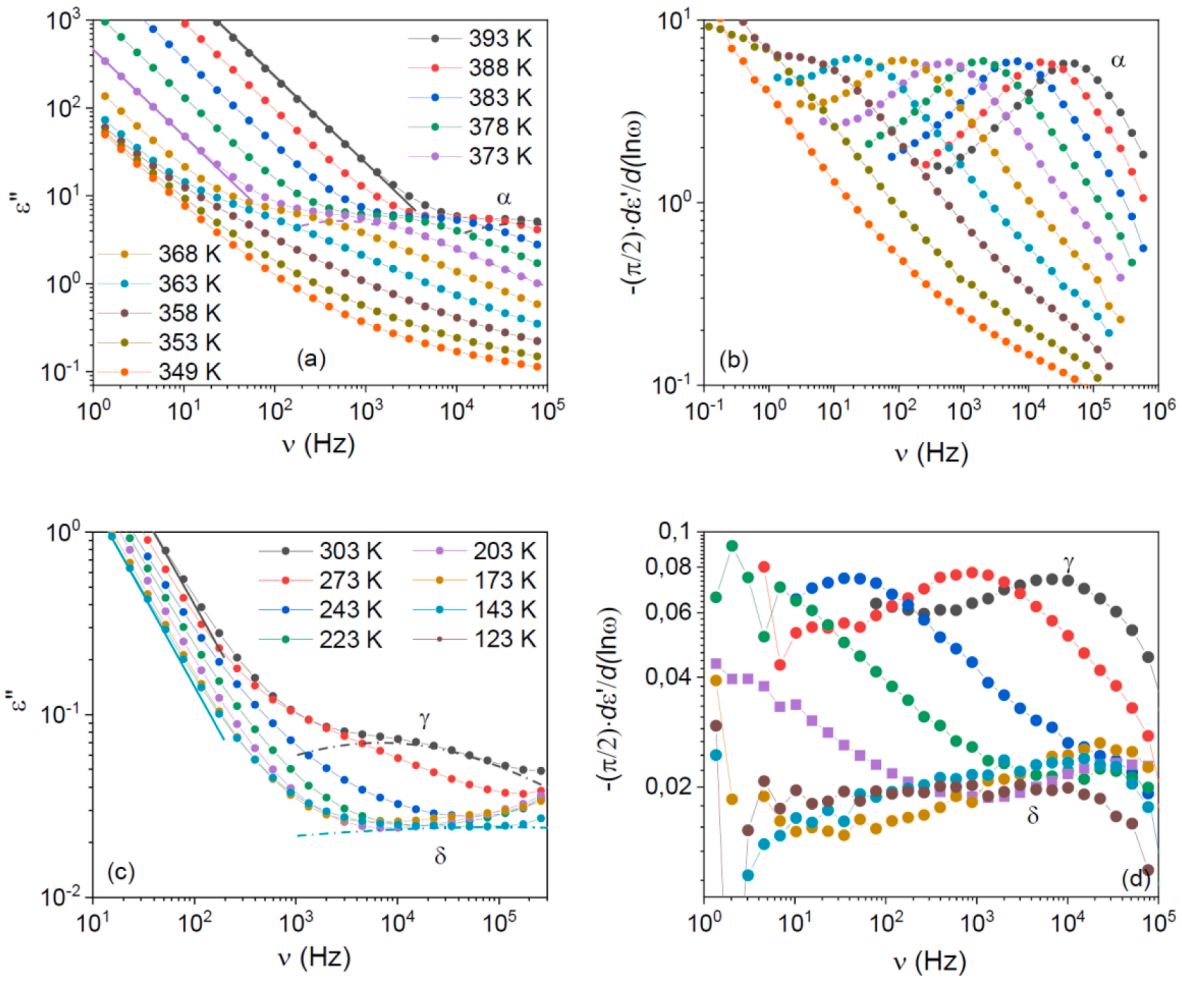

Fig. 2. Selected isothermal loss spectra of amorphous curcumin at temperatures above (a) and below T_g (c). Spectra in (a) are shown every 5 K between 349 and 393 K. Spectra in (c) are shown between 123 and 303 K, every 20 or 30 K. (b,d) Approximate dielectric loss spectra, calculated from the derivative of ε' (Eq. (3)), at the same temperatures as (a) and (c), respectively.

were fitted as the sum of several components (see Section 3.3). The fit components of representative spectra are shown in the left panels of Fig. 2.

The Arrhenius relaxation map of curcumin, resulting from the fit procedure applied to all measured spectra, is shown in Fig. 3. The slowest (and spectrally the most prominent) relaxation is the structural (α) relaxation, whose freezing-out is associated with the glass transition temperature of this compound, as detailed in what follows. In the Arrhenius plot, the structural relaxation time displayed a positive curvature as a function of the inverse temperature, which could be fitted by means of the modified Vogel-Fulcher-Tammann (VFT) equation (Angell, 1988):

$$\tau_\alpha(T) = \tau_\infty exp\left(D\frac{T_{VF}}{T - T_{VF}}\right) \quad (4)$$

Such fit yielded, for supercooled liquid curcumin, a dynamic glass transition temperature (defined as the temperature at which the structural relaxation time reaches 100 s) of 339 K, which is only slightly higher than the calorimetric T_g, and an activation energy at T_g of 708 kJ mol^{-1}. The other fit parameters are given in Table 1. The dynamic glass transition temperature is often slightly below the calorimetric one (Valenti et al., 2019). Note that also previous studies observed a significantly lower T_g than that observed by DSC (Pawar et al., 2012; Minecka et al., 2019). It is plausible that amorphous curcumin samples obtained with different methods contain different concentrations of the two tautomers (inset to Fig. 1), as suggested for example by the

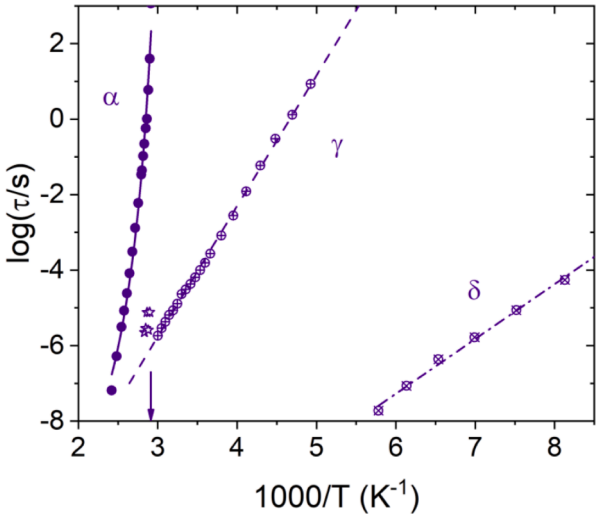

Fig. 3. Arrhenius relaxation map of amorphous curcumin. Filled circles represent the structural α relaxation, plus signs the γ relaxation, and crossed open circles the δ relaxation. Continuous lines are fits. Open stars correspond to the precursor relaxation time calculated from the Coupling Model (Eq. (6), see the text for details), while the arrow marks the position of the dynamic T_g value.

Table 1
Vogel-Fulcher-Tammann parameters and kinetic fragility of the α relaxation of curcumin, L-PADAS, D,L-PADAS, and for the dispersion of curcumin in D,L-PADAS with 30% weight fraction of curcumin.

sample	Log(τ_∞/[s]))	*D*	T_0 [K]	*m*
curcumin	–18 ± 1	16 ± 2	251 ± 6	78 ± 9
L-PADAS	–13.0 ± 0.8	8.9 ± 1.4	219 ± 5	72 ± 6
D,L-PADAS	–13.5 ± 0.6	10.1 ± 1.2	212 ± 4	72 ± 6
dispersion	–15 ± 2	13 ± 4	218 ± 11	69 ± 16

comparison of dielectric data at different pressures (Minecka et al., 2019): if the two pure tautomers have different T_g's, then it may be expected that amorphous samples obtained via different routes display different glass transition temperatures. For example, samples characterized by BDS using an increasing temperature ladder have significantly longer annealing times compared with that obtained during a DSC heating ramp, and such annealing might result in re-equilibration of the population of tautomers in the supercooled liquid.

The kinetic fragility index of the structural relaxation, a dimensionless parameter which describes the deviation of the structural relaxation from a simple Arrhenius law, is defined as (Angell, 1985; Böhmer et al., 1993):

$$m = \left.\frac{d(\mathrm{Log}\tau_\alpha)}{d(T_g/T)}\right|_{T=T_g} = \frac{DT_{VF}T_g}{(T_g - T_{VF})^2 ln10} \quad (5)$$

The second equality in Eq. (5) holds if the structural relaxation time follows the VFT Eq. (4). The dynamic fragility of curcumin is found to be 78 ± 9, in agreement with a previous study (Minecka et al., 2019).

At higher frequency than the α relaxation (or equivalently, at lower temperature) a secondary relaxation is observed, already reported in a previous study (Minecka et al., 2019) and denoted here by the symbol γ. By extending the temperature range probed, it was further possible to detect a significantly faster relaxation (labelled as δ) at lower temperature. In contrast to the structural relaxation, both secondary relaxations of curcumin were characterized by a simply-activated (Arrhenius) temperature dependence, as evidenced by the quality of the straight-line fits in both panels of Fig. 3. The γ and δ relaxations of curcumin, which were visible clearly only below T_g, have activation energies of 66 ± 5 kJ mol^{-1} and 28 ± 1 kJ mol^{-1}, respectively.

Secondary relaxations are of two types: they may correspond either to intramolecular relaxation processes (*e.g.*, interconversions between different molecular conformers, inversion dynamics of flexible rings, or reorientation of side groups) (Hellwig et al., 2020; Valenti et al., 2021), or else, they can stem from the local (sub-diffusive), whole-molecule rototranslational relaxation dynamics known as Johari-Goldstein β relaxation and which corresponds to the non-cooperative version of the molecular motion responsible for the structural relaxation (Romanini et al., 2017; Caporaletti et al., 2019). To check whether any secondary process has a Johari-Goldstein origin, Fig. 3 compares the experimental relaxation times with the predictions of the Coupling Model (Ngai, 1998; 2007). According to such model, the relaxation time of a Johari-Goldstein β at a given temperature *T* should depend exclusively on the fit parameters of the structural α relaxation at the same temperature, in particular, it should match approximately the so-called Coupling-model precursor time, which is given by (Ngai and Paluch, 2004):

$$\tau_{\mathrm{CM}}(T) = {t_c}^{1-w}{\tau_\alpha(T)}^w \quad (6)$$

here, t_c is a universal characteristic time equal to $2 \cdot 10^{-12}$ s (and valid for both molecular and macromolecular glass formers), τ_α is the structural relaxation time, and *w* is the exponent of the Kohlrausch–Williams–Watts function describing the loss feature of the α relaxation in the time domain, and which is well approximated (Alvarez et al., 1991; 1993) by $w = (ab)^{1/1.23}$, where *a* and *b* are the Havriliak-Negami exponents describing the structural loss in the frequency domain (see Section 3.3).

As it may be observed in the relaxation map of Fig. 3, the calculated precursor time τ_{CM} is relatively far (by more than one decade) from the experimental relaxation times of the γ process close to T_g, where the Coupling Model should hold, and it is extremely far from the δ_C relaxation times. Hence neither relaxation is a Johari-Goldstein β process, but rather, both secondary relaxations of curcumin arise from *intramolecular* processes, which justifies our choice of symbols. That the γ relaxation of curcumin is not a Johari-Goldstein process was already established in a previous study (Minecka et al., 2019). At the same time, tautomerism can be ruled out as a possible origin of either secondary relaxation process of curcumin: tautomeric transformation is a thermalization process that always proceeds in the same direction, not a linear response to an applied field; in fact, tautomeric transformation is observed through changes in the intensity and frequency of the structural relaxation, not as a separate relaxation process (Wojnarowska and Paluch, 2016).

Given the relative rigidity of the conjugated aryl rings of the curcumin molecule, and the lack of other dipole moments in the ethylene moiety (in order to be visible in dielectric spectroscopy, a relaxation process must involve the variation in the magnitude or orientation of the molecular dipole moment), there remain only few possible rationalizations of these intramolecular modes in terms of molecular degrees of freedom associated with a change in dipole moment. A possible origin of the relatively slow γ process of curcumin could be an interconformer relaxation dynamics between fully planar and twisted conformers. The δ relaxation is instead too fast to involve bulky functional groups, and we tentatively assign it to the coupled rotation of the hydroxyl and methoxy groups of the aromatic ring (the rotation of the methyl or non-hydrogen bonded hydroxyl groups are instead too fast to be observed in our experimental frequency window (Crossley and Smyth, 1969)). The activation energy of the δ relaxation, 28 kJ mol^{-1}, is only slightly larger than the energy of formation of an O–H…O hydrogen bond (which in water is equal to 23 mol^{-1} (Suresh and Naik, 2000). It would therefore appear that most of the activation barrier for the δ relaxation stems from the breaking of the intramolecular hydrogen bond required for the coupled methoxy-hydroxy rotation to occur.

4.2. Thermal behavior and dielectric relaxations in PADAS

Fig. 4 show the DSC traces of both L-PADAS and D,L-PADAS. The samples were first heated to their melting point, and subsequently cooled to 223 K. A second heating ramp was then performed and the melted sample was then quenched to the lowest temperature with the maximum cooling rate achievable (on average, –40 K/min). A last heating was then performed. Except for the fast quench, all other temperature ramps were performed with a heating/cooling rate of 10 K/min, and isotherms of 2 min were performed at every turning point.

L-PADAS samples behaved in agreement with previous work (Paredes et al., 1998). Double melting peaks are observed on every heating ramp ($T_{m,1}$ = 360 ± 4 K, $T_{m,2}$ = 382 ± 2 K), a feature typical of polyamides and indicative of a recrystallization process resulting in a population of smaller crystallites with lower melting point. A small cold-crystallization process could be observed before the higher melting peak. The calorimetric glass transition of the sample was observed in both heating ramps, with onset at T_g = 277 ± 1 K.

As reported in an earlier study (Paredes et al., 1998), a baseline change can be observed in the first heating around 324 K, a temperature close to the T_g of polyamides, suggesting that the amorphous part of the sample recovered from polycondensation is mostly constituted by peptidic bonds. A similar behavior was observed in D,L-PADAS samples, where the first heating ramp also presents a baseline change at 334 K. The melting behavior of D,L-PADAS resembled closely the melting of L-PADAS at high heating rates (more than 60 K/min) as measured by Paredes et al. Here, T_m = 364 ± 2 K, while the second melting peak was suppressed and no reorganization of crystals or cold-crystallization peak could be observed, in line with the single melting temperature reported

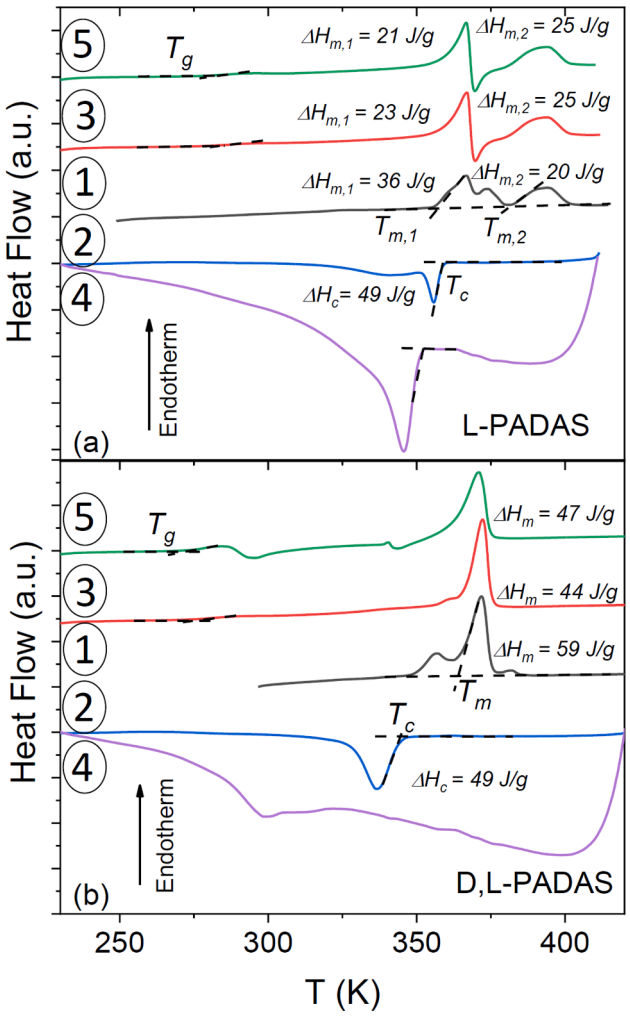

Fig. 4. DSC traces of L-PADAS (a) and D,L-PADAS (b). Lines represent: first heating at 10 K/min (black, 1), subsequent cooling at 10 K/min (blue, 2), second heating at 10 K/min (red, 3), quenching from melt at maximum speed (ca. 40 K/min, purple, 4), last heating at 10 K/min (green, 5). Phase transitions and the dynamic glass transition are indicated, as well as melting and crystallization enthalpies. (For interpretation of the references to colour in this figure legend, the reader is referred to the web version of this article.)

previously for D,L-PADAS (Rodríguez-Galán et al., 1999). The quenched sample, instead, presented a cold-crystallization peak at 288 K after the glass transition (T_g = 274 ± 1 K) (similarly to the quenched L-PADAS sample of Paredes et al.), and an additional small cold-crystallization peak at 341 K. The smaller T_g of this sample compared to L-PADAS was likely a consequence of the lower molecular weight obtained for D,L-PADAS (see Section 3.1).

It is worth stressing that the disorder imposed by the different enantiomeric ratio of D- and L-alanine was not enough to obtain a fully amorphous sample. The crystallization of neither polymer, in fact, could be avoided, even when cooling at the highest rates. The observed crystallization peaks are likely associated to the packing of polymethylene segments. The cold-crystallization temperatures T_c, as determined with a cooling rate of 10 K/min, were 358 K and 344 K for L-PADAS and D,L-PADAS, respectively. More than in the glass transition temperature, the enantiomeric disorder was reflected in the crystallization temperature, which is 14 K lower for D,L-PADAS. The crystallinity of the samples was calculated supposing an enthalpy of fusion for the 100% crystalline sample of 173 J/g (or equivalently 88 kJ mol^{-1}, considering the molar mass of the repeating unit (Paredes et al., 1998)). Both polymers recovered from polymerization had a crystallinity of approximately 33 %, in agreement with previous findings and only slightly higher than the crystalline fraction achieved after cooling from the melt, which was approximately 28 %.

Selected dielectric spectra of the PADAS samples are shown in Fig. 5. All spectra were fitted applying the procedure detailed in Section 3.3. Four main relaxations can be observed in the spectra of both polymers, of which two, labelled as α and MW, were observed for temperatures near or higher than the T_g of the corresponding samples, and two more, labelled β and γ in the loss spectra, are observed in the glass state. The fit components of representative spectra are displayed in Fig. 5.

The Arrhenius plot of these four relaxations in both L-PADAS and D, L-PADAS are shown in Fig. 6(a). It may be observed that the relaxation times are very similar in both copolymers, and that for the α and MW processes the temperature dependence of the relaxation times depart from a simply activated behavior. The α relaxation time could be modeled with a VFT function (Eq. (4)). The VFT fit parameters of both samples are reported in Table 1, together with the fragility value (see Eq. (5)). The enantiomeric ratio of D and L-alanine does not affect the fragility of the polymer, since *m* is basically the same in both cases (72 ± 6). This can also be evidenced by the Angell plot of the low-frequency relaxations of both copolymers, displayed in Fig. 6(b).

The dynamic T_g, defined also for the polymer samples as the temperature at which $\tau_\alpha = 100$ s, was 276 ± 1 K for L-PADAS and 272 ± 1 K for D,L-PADAS, respectively. Both temperatures are in agreement with the DSC results, which indicates that the α process corresponds to the structural (segmental) relaxation of the polymers. The α relaxation was modelled as a Havriliak-Negami function, and its dielectric strength and low-frequency value of the real permittivity were in line with those expected for a polymer sample. On the other hand, the MW process had significantly higher dielectric strength (see panels (a) and (c) of Fig. 5) and a Cole-Cole lineshape. The high dielectric strength excludes the possibility that this relaxation may correspond to a normal mode of the polymer (Ren et al. (2003)). Moreover, the frequency of normal modes should depend on the molecular weight of the polymer chains, while its curvature in the Arrhenius plot should remain constant. These effects are not observed in Fig. 6, despite the difference in molecular weight between the D,L-PADAS and L-PADAS polymers.

These observations suggest an interfacial origin of the MW relaxation, related to the heterogeneous nature of the sample. In phase separated samples, containing for example a crystalline and an amorphous fraction or else a phase separation between two immiscible phases, so-called Maxwell-Wagner relaxations arise (Wagner, 1914), which are due to accumulation of bound and/or free charge at the interphase separation and which usually display a relatively narrow Cole-Cole lineshape (Zachariah et al., 2015; Valenti et al., 2020). This justifies our choice of the label "MW" to indicate the slowest observed dielectric relaxation. An obvious source of heterogeneity in our polymer samples comes from their semicrystalline nature, so that one may be tempted to ascribe the MW process of PADAS to charge accumulation at the amorphous-crystalline boundary. However, as it will be shown in Section 4.3, the MW relaxation is present also in fully amorphous dispersions of curcumin in PADAS, which rules out this hypothesis. We therefore ascribe the interfacial MW process to an intrinsic nanophase segregation of the PADAS polymer (which is actually a *co*polymer) into regions of distinct average chemical composition. For example, the synthesized PADAS chains contain relatively long lipophilic hydrocarbon chains, which constitute the backbone of both sebacic acid and dodecanodiol components, which might tend to phase-segregate from more hydrophilic regions containing their endgroups and the alanine monomers. A similar interfacial relaxation in a copolymer was recently reported in chain-extended polylactide (Yousefzade et al., 2019).

Concerning the secondary processes visible below T_g, close inspection of the data for the β relaxation of the copolymers reveals that τ_β coincides with predictions from the Coupling Model (Eq. (6)), represented as blue stars in Fig. 6(b). Moreover, this relaxation displays a slight change of activation energy at T_g, which is typical of Johari-

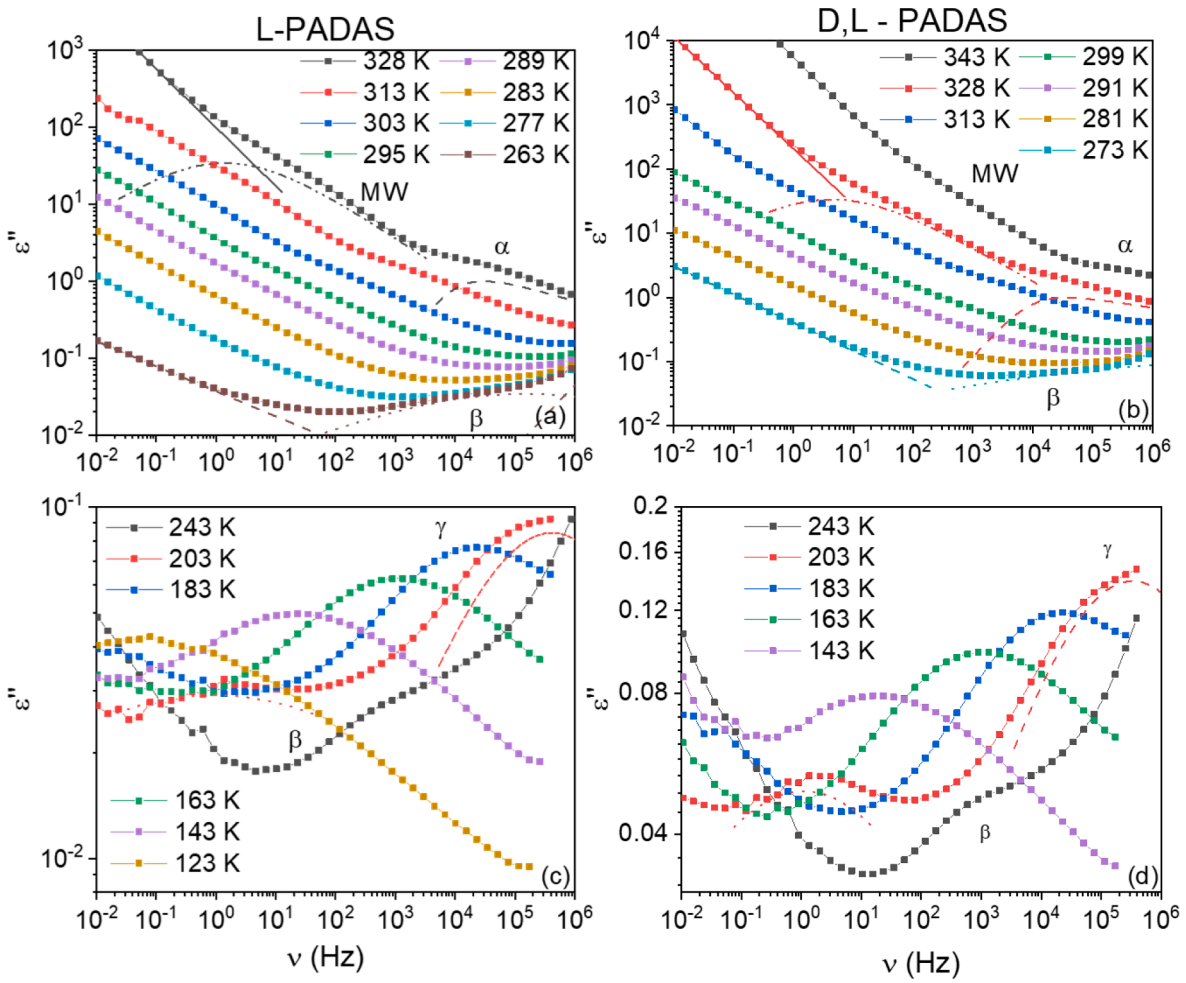

Fig. 5. Dielectric loss spectra of L-PADAS (a,b) and D,L-PADAS (c,d) as a function of frequency, for selected temperatures. Dashed and dotted curves are fit components, shown only for selected spectra.

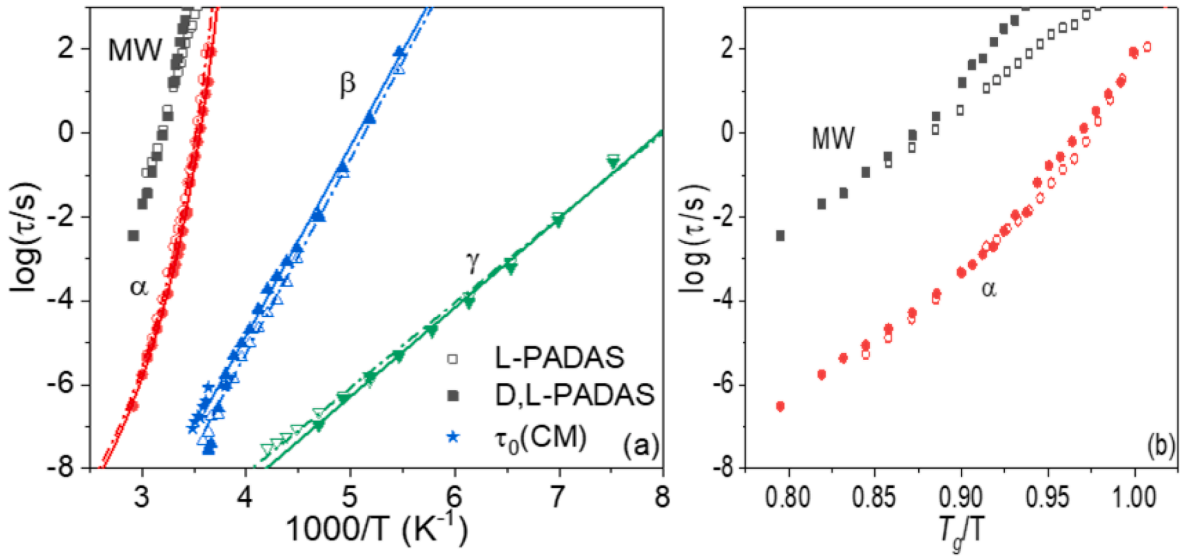

Fig. 6. (a) Arrhenius relaxation map of L-PADAS (open markers) and D,L-PADAS (filled markers), corresponding to the series of dielectric spectra of which a selection is shown in Fig. 5. Blue stars are the predicted precursor relaxation times according to the Coupling Model Eq. (6). (b) Angell plot of the α and MW relaxations of the same samples. (For interpretation of the references to colour in this figure legend, the reader is referred to the web version of this article.)

Goldstein intermolecular relaxations (Ngai and Paluch, 2004). On the other hand, the γ relaxation of PADAS, which is characterized by an activation energy of 39 ± 1 kJ mol^{-1}, must stem from a local relaxation process. This process has very similar relaxation time and basically the same activation energy as the local secondary relaxation dynamics of polycaprolactone, a polyester (Christodoulou et al., 2020). The only group presenting an electric dipole and common to both polymers is the ester group, which leads us to assign the γ relaxation of PADAS to a local configurational reorientation of the ester group, possibly associated to a torsional rotation of (part of) the chains around a backbone C − O bond.

4.3. Binary dispersions

Fig. 7 displays DSC traces of the first (panel (a)) and second (panel (b)) heating ramp of dispersions of curcumin in D,L-PADAS, for different weight fractions of curcumin. For comparison purposes, also the DSC traces of curcumin and D,L-PADAS are shown. The first heating curves of the binary mixtures (panel (a)) reveal that the as-casted samples are semicrystalline, as they display both step-like baseline changes typical of the glass transition, and melting peaks. The temperatures of the double melting feature were lower with higher curcumin concentration, a typical behavior of binary samples. The overall intensity of melting features, which represents the enthalpy of transition, decreased with increasing curcumin concentration. This indicates that the as-casted binary samples likely had lower crystalline fraction than pure D,L-PADAS.

No crystallization is observed upon cooling, so that the samples were fully amorphous at the beginning of the second heating ramp. Cold crystallization was observed only at relatively low curcumin concentrations, namely up to a concentration of 23 wt%. The mixtures with 30 and 50 wt% of curcumin did not show any sign of cold-crystallization or melting, and the sample recovered after the second heating ramp was completely amorphous. In all second-heat ramps, only one glass transition was observed, indicative of samples without amorphous phase separation (the T_g feature in the first heating curve was generally different than that of the second heating, which shows that as-casted films were not compositionally homogeneous and that homogeneity improved upon melting).

The 30 and 50 wt% mixtures were completely amorphous and homogeneous after the first melting. Curcumin has a clear antiplasticizing effect (Valenti et al., 2022) on the polymer, as the T_g of the mixtures increased with increasing curcumin content. The concentration dependence of the T_g of the mixtures (as determined from the second heat-up DSC scan) could be well modelled (see Fig. 7(c)) with the Gordon-Taylor equation (Gordon and Taylor, 1952):

$$T_{g,ASD} = \frac{(1-x)T_{g,PADAS} + KxT_{g,curcumin}}{1-x+Kx} \quad (7)$$

The dimensionless constant K, which accounts for the slight curvature observed in the dependence of T_g with weight composition of the dispersion, is found to be equal to 1.1 ± 0.1, which means that T_g is roughly linearly proportional to concentration, as observed. Indeed, a linear fit (not shown) also provides a good approximation to the experimental data, with a regression coefficient $r^2 = 0.9986$.

The fully amorphous dispersion at 30 wt% of curcumin in D,L-PADAS was selected to investigate the relaxation dynamics of the binary system. Fig. 8 displays dielectric loss data of this dispersion. The isochronal plot of the dielectric loss at selected frequencies (Fig. 8(d)), reveals the presence of two relaxations above T_g, labeled as α and MW, and three relaxations below T_g (which are labeled as γ, γ' and β from the fastest to the slowest). Selected dielectric loss spectra as a function of frequency are presented in panels (a) and (c). The fit components of representative spectra are shown in the same panels. At high temperatures, the contribution of the conductivity and an electrode polarization are discerned in the spectra, and these relatively strong contributions mask partially the presence of the MW relaxation, which is however

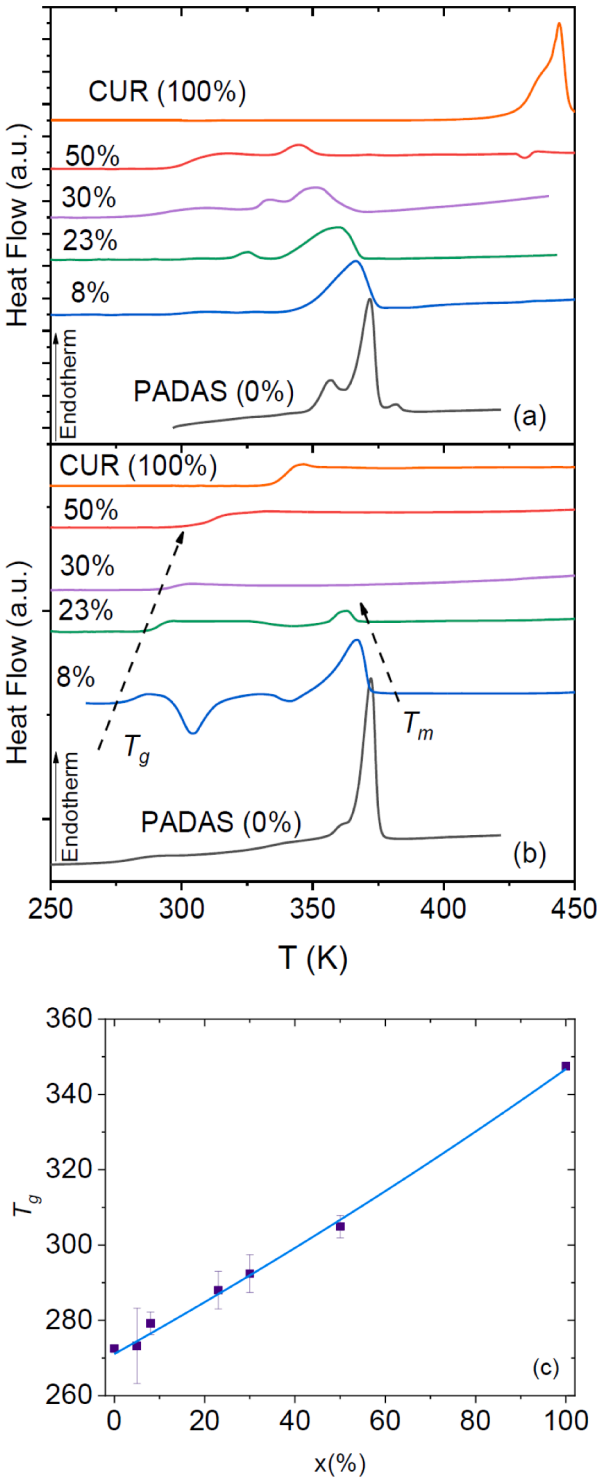

Fig. 7. (a,b) DSC traces of L,D-PADAS and curcumin, and of their binary mixtures at different curcumin weight percentages as indicated. First (a) and second (b) heating ramps are presented. The glass transition, melting and cold-crystallization temperatures are indicated. (c) T_g of binary mixtures plotted against the weight composition of curcumin. Error bars indicate the reliability of the identification of the position of the T_g feature in the second heating ramps of panel (b). The solid line is a fit with the Gordon-Taylor Eq. (7).

confirmed by our fit procedure. The presence of this relaxation also in the binary dispersion is visually confirmed by the ohmic-loss-free dielectric loss calculated from the derivative of ε′ (see Eq. (3)), displayed in panel (b), where it gives rise to a very intense feature on the

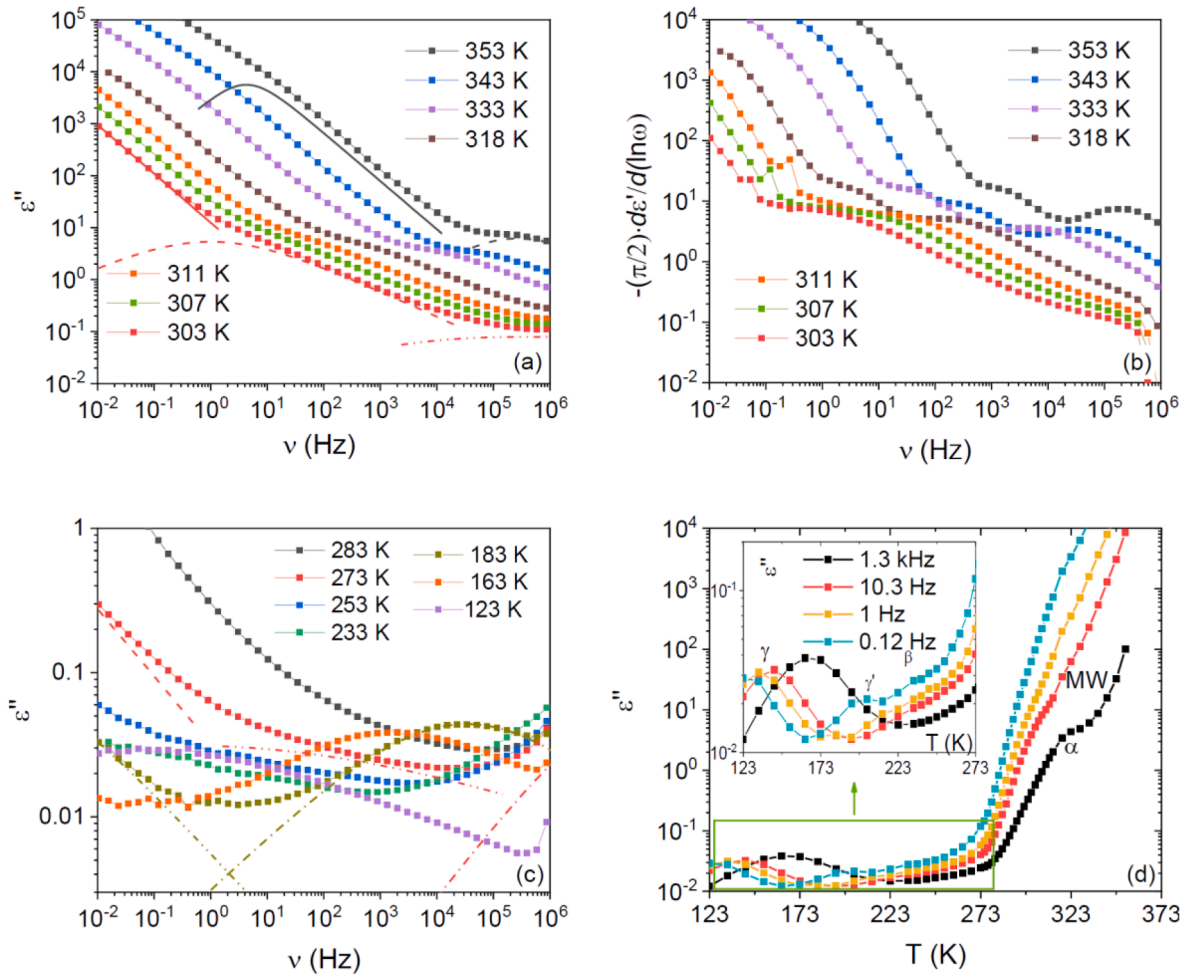

Fig. 8. (a,c) Dielectric loss spectra of the homogeneous amorphous dispersion of curcumin in D,L-PADAS at 30% weight content of the bioactive molecule, for selected temperatures above (a) and below (c) T_g. (b): Derivative dielectric loss spectra (Eq. (3)) corresponding to the loss spectra as in (a). (d) Isochronal loss spectra of the sample at selected fixed frequencies (see legend). Inset: zoom-in of the low-temperature portion of the curves in the main panel.

low-frequency side of the α relaxation. The secondary relaxations are clearly visible directly in the low temperature dielectric loss spectra (panel (c)).

The Arrhenius plot of all relaxations of the binary dispersion are displayed in Fig. 9(a), where the data for pure amorphous curcumin and pure D,L-PADAS are also plotted for comparison purposes. For better clarity, the secondary relaxations of pure curcumin are labeled as γ_C and δ_C in the legend. The temperature-dependent α relaxation times of the binary dispersion could be fitted with a VFT function. The fit parameters are listed in Table 1. The dynamic T_g of the mixture (290 ± 3 K) is in between those of the pure components and in agreement with the calorimetric T_g determinations. The fragility index of the dispersion was virtually identical to that of the pure polymer (see Table 1), and indeed the the α relaxation times of the dispersion coincide with the relaxation times of D,L-PADAS in the Angell plot (inset to Fig. 9(b)), suggesting that the primary relaxation is governed by the polymer chains also in the binary mixture.

As visible in Fig. 9(a), while the primary α relaxation times are strongly modified by addition of the curcumin antiplasticizer, the MW relaxation is barely affected by the presence of curcumin molecules, which might be expected for a relaxation that stems from nanophase segregation of the polymer component. In fact, the MW relaxation is actually slightly faster when curcumin is added (while the α relaxation slows down due to the antiplasticizing effect). This might indicate that the nanophase segregation of the polymer chains into (lipophilic and hydrophilic) domains, or the conductivity and/or static permittivity of each nanophase, is different in the binary mixture than in the pure polymer. Curcumin is known to form hydrogen bonds (Minecka et al., 2019), so that its presence is likely to alter the pristine interactions between the chains in pure PADAS.

The β relaxation of the binary dispersion can be safely identified with a Johari-Goldstein relaxation. This is confirmed both by the observation of a sharp dynamic cross-over of this relaxation (change of activation energy) near T_g, and by comparison with the prediction of the Coupling Model (Fig. 9(a)). Concerning the other two secondary processes in the dispersion, they cannot correspond to the Johari-Goldstein process of nanoconfined curcumin (Ruiz et al., 2019; Ngai et al., 2019, Ngai et al. (2020)), as testified by the poor comparison with the Coupling Model prediction for pure curcumin, but must have an intramolecular origin. Previous studies have shown that intramolecular relaxations of small-molecule glass formers are not influenced by the local environment in the liquid or amorphous phase, and their relaxation times in different samples are superposed in the Arrhenius plot (Romanini et al., 2021; Valenti et al., 2019, 2021); however, in the case of polymer secondary relaxations, this is not always the case, and a study via an Angell plot may be more suited to identify the relaxation processes and analyze the effect of dilution of a component in a polymer dispersion (Romanini et al., 2018).

In the present case, no clear information about the nature of intramolecular processes of the dispersion can be gathered from the Arrhenius plot of Fig. 9(a), while the Angell plot of Fig. 9(b) is most informative: for example, the γ relaxation of the dispersion coincides

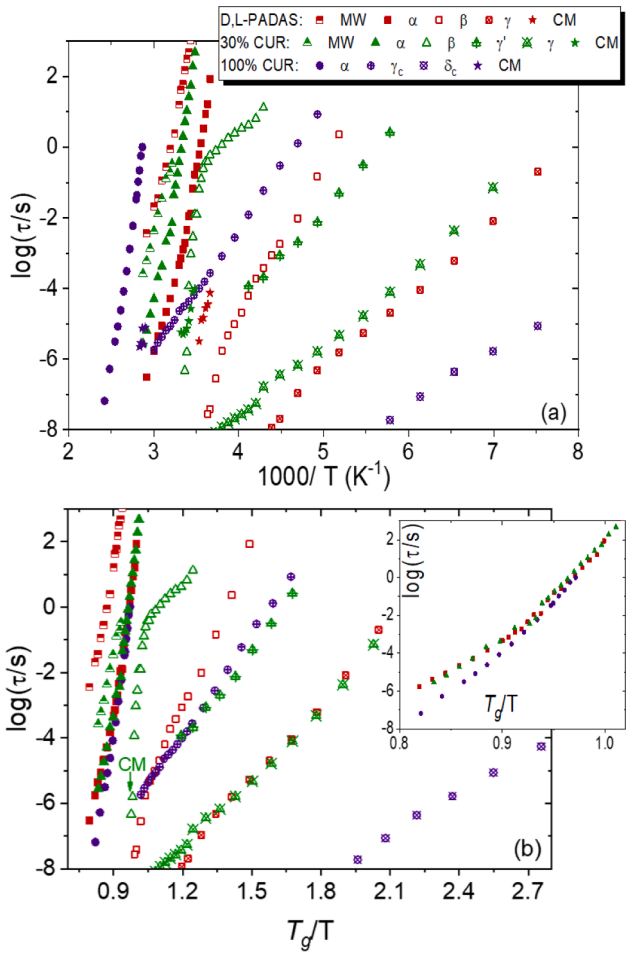

Fig. 9. Arrhenius (a) and Angell (b) plot of the amorphous binary mixture (green), compared with pure D,L-PADAS (red) and pure curcumin (purple). Inset to (b): Angel plot of only the α relaxation. (For interpretation of the references to colour in this figure legend, the reader is referred to the web version of this article.)

with that of the pure polymer in the Angell plot. This allows identifying the γ relaxation of the dispersion with the rotation of ester groups, as in the case of pure PADAS. Similarly, in the Angell representation the γ' relaxation times of the binary mixture are superposed with those of the γ_C relaxation of pure curcumin, which confirms that they are the same process. The Angell plot scaling of these secondary relaxation times with T_g moreover shows that both internal relaxation modes are actually affected by the viscosity of the sample. A similar behavior was reported previously for a secondary polymer relaxation in dispersions of a drug in poly(vinylpyrrolidone) (Romanini et al., 2018). On the other hand, the faster and weaker secondary (δ) relaxation of pure curcumin is not observed, likely due to its too low intensity when curcumin is diluted in the polymer.

4.4. Controlled release of curcumin from PADAS dispersions

The controlled release of curcumin from its 30 wt% dispersion in PADAS was studied in a Simulated Body Fluid (SBF) at 310 K. The result of the control-release characterization is shown in Fig. 10. The release rate was studied initially in the pure SBF during 48 h; after this time, ethanol was added to the release medium to check that the polymer carrier still contained an appreciable amount of drug. It can indeed be seen that the amount of released drug increased dramatically upon addition of ethanol. The sudden surge of the drug concentration (i.e., of the release rate) in the ethanol solution is most likely due to the swelling

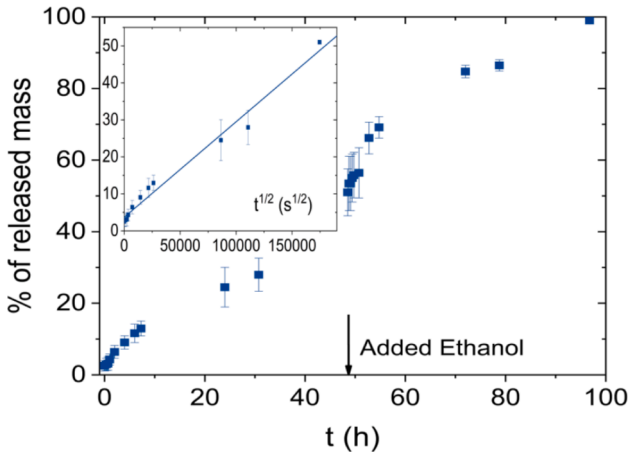

Fig. 10. Release curve for the 30% amorphous dispersion of curcumin in PADAS, in a Simulated Body Fluid (SBF) at human body temperature (310 K), both before and after addition of ethanol in a relative ratio of 3 to 1. The curve represents the mass percentage of the total initial curcumin content that is present in solution after time *t*. Inset: release curve in pure SBF (without ethanol) plotted as a function of the square root of the time elapsed since the beginning of the experiment. Markers with error bars are experimental points, while the continuous line is a linear fit. In both the main figure and in the inset, the results are the average of five replicates, and error bars represent standard deviations.

of the polymer in ethanol (while it is insoluble in water).

It is observed in Fig. 10 that the percentage of drug released in the SBF increased quite fast at short times and then reached an equilibrium value of about 51% of the total initial curcumin content after 48 h. This percentage is significantly higher than the corresponding value in dispersions in simple polyesters (Valenti et al., 2019). The inset to Fig. 10 shows that the amount of curcumin released in the simulated body fluid is linearly proportional to the square root of time ($t^{1/2}$). This behavior agrees with the prediction of simple Fickian diffusion in a thin polymer sample (Siepmann and Peppas, 2011) and with the so-called Higuchi model (Higuchi, 1963), which describes the release in a medium as $Q(t) = K_H\, t^{1/2}$ where $Q(t)$ is the cumulative amount of drug released after time *t*. In the diffusivity-based models that predict a $t^{1/2}$ dependence, the constant K_H is proportional to the square root of the diffusivity. In the present case, the constant is found to be $K_H = (2.6 \pm 0.2)\cdot 10^{-4}$ $s^{-1/2}$.

Drug release from poly(ester amide) matrices may display also a long-term "erosional" phase due to degradation of PADAS molecules, just as is the case for polyesters like polylactide, which generally exhibit a second burst in the release after 4–5 months. This long-term, erosion-induced release lies outside the scope of the present contribution.

5. Conclusions

Differential scanning calorimetry and broadband dielectric spectroscopy were employed to investigate the glass transition and (macro) molecular relaxation dynamics of amorphous curcumin, a biodegradable semicrystalline poly(ester amide) (PADAS), and amorphous dispersions of curcumin in such copolymer. Supercooled liquid curcumin displayed, besides the structural relaxation visible above its glass transition temperature T_g, two secondary relaxations visible below T_g. The secondary relaxations are tentatively assigned to specific molecular motions: a conformational change involving the orientation of the two relatively rigid arms of the molecule, with an activation energy of 66 ± 5 kJ mol^{-1}, and the coupled rotation of the hydroxyl and methoxy groups of the aromatic ring, with activation energy of 28 ± 1 kJ mol^{-1}. The poly(ester amide) also displayed two secondary relaxations below its T_g, one of which corresponded to the Johari-Goldstein mode, while the other one, of activation energy of 39 ± 1 kJ mol^{-1}, is assigned to a

torsional rotation of short chain segments around a backbone C − O bond. Besides these two secondary relaxations and the primary relaxation associated with the T_g of the polymer, PADAS also exhibited a Maxwell-Wagner relaxation, whose likely origin are spatial heterogeneities associated with amorphous phase disproportionation in this polymer.

In order to increase the kinetic stability of amorphous curcumin, solid dispersion of this biologically active molecule in PADAS were investigated. Binary dispersions with curcumin mass fraction between 30 and 50% were completely amorphous, and displayed a single structural relaxation and a single Johari-Goldstein relaxation. Both the torsional rotation of the ester groups of PADAS and the conformational relaxation of curcumin were observed in the amorphous dispersions. The relaxation times of both processes overlapped with those of the pure components in the Angell plot. Such scaling with the T_g of the mixture is an indication that these secondary processes are sensitive to the viscosity of the surrounding matrix. The release of curcumin from its dispersion at 30% in mass percent in PADAS was studied in a simulated body fluid at human body temperature. The release profile followed the diffusive Higuchi model with Higuchi constant equal to $K_H = (2.6 \pm 0.2)\cdot 10^{-4}$ $s^{-1/2}$. In 48 h, 51% of the initial curcumin content of the binary dispersion was released. This is a significantly higher fraction compared to those obtained in release experiments from simple polyesters, and suggests a possible pharmacological use of the curcumin dispersions in PADAS.

Author contributions

The manuscript was written through contributions of all authors. All authors have given approval to the final version of the manuscript.

Declaration of Competing Interest

The authors declare that they have no known competing financial interests or personal relationships that could have appeared to influence the work reported in this paper.

Data availability

Data will be made available on request.

Acknowledgments

This research was funded by the Spanish Ministry of Economy and Competitiveness MINECO through projects PID2020-112975 GB-I00 and PID2022-140302OB-I00, and by the Generalitat de Catalunya under the projects 2021SGR-00343 and 2021SGR-01042.

References

Aggarwal, B.B., Gupta, S.C., Sung, B., 2013. Curcumin: an orally bioavailable blocker of TNF and other pro-inflammatory biomarkers. Brit. J. Pharmacol. 169, 1672–1692.
Aggarwal, B.B., Sung, B., 2009. Pharmacological basis for the role of curcumin in chronic diseases: An age-old spice with modern targets. Trends Pharmacol. Sci. 30, 85–94.
Ak, T., Gülçin, I., 2008. Antioxidant and radical scavenging properties of curcumin. Chem. Biol. Interact. 174, 27–37.
Alvarez, F., Alegría, A., Colmenero, J., 1991. Relationship between the time-domain kohlrausch-williams-watts and frequency-domain havriliak-negami relaxation functions. Phys. Rev. B 44, 7306–7312.
Alvarez, F., Alegría, A., Colmenero, J., 1993. Interconnection between frequency-domain havriliak-negami and time-domain kohlrausch-williams-watts relaxation functions. Phys. Rev. B 47, 125–130.
Anand, P., Kunnumakkara, A.B., Newman, R.A., Aggarwal, B.B., 2007. Bioavailability of curcumin: Problems and promises. Mol. Pharm. 4, 807–818.
Angell, C.A., 1985. Spectroscopy simulation and scattering, and the medium range order problem in glass. J. Non Cryst. Solids 73, 1–17.
Angell, C.A., 1988. Structural instability and relaxation in liquid and glassy phases near the fragile liquid limit. J. Non Cryst. Solids 102, 205–221.
Barrio, M., Espeau, P., Tamarit, J.L., Perrin, M., Veglio, N., Céolin, R., 2009. Polymorphism of progesterone: Relative stabilities of the orthorhombic phases I and II inferred from topological and experimental pressure-temperature phase diagrams. J. Pharm. Sci. 98, 1657–1670.
Bar-Sela, G., Epelbaum, R., Schaffer, M., 2010. Curcumin as an anticancer agent: review of the gap between basic and clinical applications. Curr. Med. Chem. 17, 190–197.
Bhardwaj, S., Arora, K., Kwong, E., Templeton, A., Clas, S., Suryanarayanan, R., 2013. Correlation between molecular mobility and physical stability of amorphous itraconazole. Mol. Pharm. 10, 694–700.
Böhmer, R., Ngai, K.L., Angell, C.A., Plazek, D.J., 1993. Nonexponential relaxations in strong and fragile glass formers. J. Chem. Phys. 99, 4201–4209.
Caporaletti, F., Capaccioli, S., Valenti, S., Mikolasek, M., Chumakov, A.I., Monaco, G., 2019. A microscopic look at the Johari-Goldstein relaxation in a hydro-gen-bonded glass-former. Sci. Rep. 9, 14319.
Christodoulou, E., Klonos, P.A., Tsachouridis, K., Zamboulis, A., Kyritsis, A., Bikiaris, D. N., 2020. Synthesis, crystallization, and molecular mobility in poly (ε-caprolactone) copolyesters of different architectures for biomedical applications studied by calorimetry and dielectric spectroscopy. Soft Matter 16, 81878201.
Cole, R.H., Cole, K.S., 1942. Dispersion and absorption in dielectrics II. Direct Current Characteristics. *J. Chem. Phys.* 10, 98.
Crossley, J., Smyth, C.P., 1969. Microwave absorption and molecular structure in liquids. LXXIII. A dielectric study of solute-solvent interactions. J. Am. Chem. Soc. 91, 10, 2482–2487.
De, R., Kundu, P., Swarnakar, S., Ramamurthy, T., Chowdhury, A., Nair, G.B., Mukhopadhyay1, A.K., 2009. Antimicrobial activity of curcumin against Helicobacter pylori isolates from India and during infections in mice. Antimicrob. Agents Chemother. 53, 1592–1597.
Del Valle, L.J., Roca, D., Franco, L., Puiggalí, J., Rodríguez-Galán, A., 2011. Preparation and release study of ibuprofen-loaded porous matrices of a biodegradable poly (ester amide) derived from L-alanine units. J. Appl. Polym. Sci. 122, 1953–1967.
Del Valle, L.J., Roa, M., Díaz, A., Casas, M.T., Puiggalí, J., Rodríguez-Galán, A., 2012. Electrospun nanofibers of a degradable poly (ester amide). Scaffolds loaded with antimicrobial agents. J. Polym. Res. 19, 1–13.
Dhillon, N., Aggarwal, B.B., Newman, R.A., Wolff, R.A., Kunnumakkara, A.B., Abbruzzese, J.L., Ng, C.S., Badmaev, V., Kurzrock, R., 2008. Phase II trial of curcumin in patients with advanced pancreatic cancer. Clin. Cancer Res. 14, 4491–4499.
Fonseca, A.C., Gil, M.H., Simões, P.N., 2014. Biodegradable poly(ester amide)s – A remarkable opportunity for the biomedical area: Review on the synthesis, characterization and applications. Prog. Polym. Sci. 39, 1291–1311.
Gordon, M., Taylor, J.S., 1952. Ideal copolymers and the second-order transitions of synthetic rubbers. I. Non- Crystalline Copolymers. *J. Appl. Chem.* 2, 493–500.
Gupta, P., Chawla, G., Bansal, A., 2004. Physical stability and solubility advantage from amorphous celecoxib: The role of thermodynamic quantities and molecular mobility. Mol. Pharm. 1, 406–413.
Han, S., Wu, J., 2022. Recent advances of poly(ester amide)s-based biomaterials. Biomacromolecules 23, 1892–1919.
Havriliak, S., Negami, S.A., 1967. Complex plane representation of dielectric and mechanical relaxation processes in some polymers. Polymer 8, 161–210.
Hellwig, H., Nowok, A., Małecki, J.G., Kuś, P., Jędrzejowska, A., Grzybowska, K., Pawlus, S., 2020. Conformational analysis and molecular dynamics of glass-forming aromatic thiacrown ethers. PCCP 22, 17948–17959.
Higuchi, T., 1963. Mechanism of sustained-action medication. Theoretical analysis of rate of release of solid drugs dispersed in solid matrices. J. Pharm. Sci. 52, 1145–1149.
Kissi, E.O., Grohganz, H., Löbmann, K., Ruggiero, M.T., Zeitler, J.A., Rades, T., 2018. Glass-transition temperature of the β-relaxation as the major predictive parameter for recrystallization of neat amorphous drugs. J. Phys. Chem. B 122, 2803.
Liechty, W.B., Kryscio, D.R., Slaughter, B.V., Peppas, N.A., 2010. Polymers for drug delivery systems. Annu. Rev. Chem. Biomol. Eng. 1, 149–173.
Minecka, A., Kamińska, E., Heczko, D., Jurkiewicz, K., Wolnica, K., Dulski, M., Hachuła, B., Pisarski, W., Tarnacka, M., Talik, A., Kamiński, K., Paluch, M., 2019. Studying structural and local dynamics in model H-bonded active ingredient - Curcumin in the supercooled and glassy states at various thermodynamic conditions. Eur. J. Pharm. Sci. 135, 38–50.
Ngai, K.L., 1998. Relation between some secondary relaxations and the α relaxations in glass-forming materials according to the coupling model. J. Chem. Phys. 109, 6982.
Ngai, K.L., 2007. Why the glass transition problem remains unsolved? J. Non Cryst. Solids 353, 709–718.
Ngai, K.L., Paluch, M., 2004. Classification of secondary relaxation in glass-formers based on dynamic properties. J. Chem. Phys. 120, 857–873.
Ngai, K.L., Lunkenheimer, P., Loidl, A., 2019. Predicting the α-relaxation time of glycerol confined in 1.16 nm pores of zeolitic imidazolate frameworks. PCCP 22, 507–511.
Ngai, K.L., Wojnarowska, Z., Paluch, M., 2020. The structural α-relaxation times of prilocaine confined in 1 nm pores of molecular sieves: Quantitative explanation by the coupling model. PCCP 22, 9257.
Paredes, N., Rodriguez-Galan, A., Puiggali, J., Peraire, C., 1998. Studies on the biodegradation and biocompatibility of a new poly (ester amide) derived from L-alanine. J. Appl. Polym. Sci. 69, 1537–1549.
Pawar, Y.B., Shete, G., Popat, D., Bansal, A.K., 2012. Phase behavior and oral bioavailability of amorphous curcumin. Eur. J. Pharm. Sci. 47, 56–64.
Priyadarsini, K.I., 2014. The chemistry of curcumin: From extraction to therapeutic agent. Molecules 19, 20091–20112.
Ren, J., Urakawa, O., Adachi, K., 2003. Dielectric and viscoelastic studies of segmental and normal mode relaxations in undiluted poly(d, l-lactic acid). Macromolecules 36, 210.
Rodriguez-Galan, A., Franco, L., Puiggalí, J., 2011. Degradable Poly(ester amide)s for biomedical applications. Polymers 3, 65–99.

Rodríguez-Galán, A., Pelfort, M., Aceituno, J., Puiggalí, J., 1999. Comparative studies on the degradability of poly(ester amide)s derived from l- and l, d-alanine. J. Appl. Polym. Sci. 74, 2312–2320.
Romanini, M., Barrio, M., Macovez, R., Ruiz-Martin, M.D., Capaccioli, S., Tamarit, J.L., 2017. Thermodynamic scaling of the dynamics of a strongly hydrogen-bonded glass-former. Sci. Rep. 7, 1346.
Romanini, M., Lorente, M., Schammé, B., Delbreilh, L., Dupray, V., Coquerel, G., Tamarit, J.L., Macovez, R., 2018. Enhancement of the physical and chemical stability of amorphous drug-polymer mixtures via cryogenic comilling. Macromolecules 51, 9382–9392.
Romanini, M., Macovez, R., Barrio, M., Tamarit, J.L., 2021. Inter-enantiomer conversion dynamics and johari-goldstein relaxation of benzophenones. Sci. Rep. 11, 20248.
Ruiz, G.N., Combarro-Palacios, I., McLain, S.E., Schwartz, G.A., Pardo, L.C., Cerveny, S., Macovez, R., 2019. Tuning molecular dynamics by hydration and confinement: Antiplasticizing effect of water in hydrated prilocaine nanoclusters. PCCP 21, 15576–15583.
Sanphui, P., Bolla, G., 2018. Curcumin, a biological wonder molecule: A crystal engineering point of view. Cryst. Growth Des. 18, 5690–5711.
Sanphui, P., Goud, N.R., Khandavilli, U.B.R., Bhanoth, S., Nangia, A., 2011. New polymorphs of curcumin. Chem. Commun. 47, 5013–5015.
Siepmann, J., Peppas, N.A., 2011. Higuchi equation: Derivation, applications, use and misuse. Int. J. Pharm. 418, 612.
Srinivasan, K., 2014. Antioxidant potential of spices and their active constituents. Crit. Rev. Food Sci. 54, 352–372.
Suresh, S.J., Naik, V.M., 2000. Hydrogen bond thermodynamic properties of water from dielectric constant data. J. Chem. Phys. 113, 9729–9732.
Szczurek, J., Rams-Baron, M., Knapik-Kowalczuk, J., Antosik, A., Szafraniec, J., Jamróz, W., Dulski, M., Jachowicz, R., Paluch, M., 2017. Molecular dynamics, recrystallization behavior, and water solubility of the amorphous anticancer agent bicalutamide and its polyvinylpyrrolidone mixtures. Mol. Pharm. 14, 4.
Thorat, A.A., Dalvi, S.V., 2015. Solid-state phase transformations and storage stability of curcumin polymorphs. Cryst. Growth Des. 15, 1757–1770.
Valenti, S., Diaz, A., Romanini, M., del Valle, L.J., Puiggalí, J., Tamarit, J.L., Macovez, R., 2019. Amorphous binary dispersions of chloramphenicol in enantiomeric pure and racemic poly-lactic acid: Morphology, molecular relaxations, and controlled drug release. Int. J. Pharmaceutics 568, 118565.
Valenti, S., Yousefzade, O., Puiggalí, J., Macovez, R., 2020. Phase-selective conductivity enhancement and cooperativity length in PLLA/TPU nanocomposite blends with carboxylated carbon nanotubes. Polymer 191, 122279.
Valenti, S., Barrio, M., Negrier, P., Romanini, M., Macovez, R., Tamarit, J.L., 2021. Comparative physical study of three pharmaceutically active benzodiazepine derivatives: Crystalline versus amorphous state and crystallization tendency. *Mol. Pharmaceutics* 18, 1819–1832. *ibid.* 3926–3927.
Valenti, S., del Valle, L.J., Romanini, M., Mitjana, M., Puiggalí, J., Tamarit, J.L., Macovez, R., 2022. Drug-biopolymer dispersions: morphology- and temperature-dependent (Anti)plasticizer effect of the drug and component-specific johari-goldstein relaxations. Int. J. Mol. Sci. 23, 2456.
Wagner, K.W., 1914. Erklärung der dielektrischen nachwirkungsvorgänge auf grund maxwellscher vorstellungen. Arch. Electrotech. 2, 371. https://doi.org/10.1007/BF01657322.
Winnacker, M., Rieger, B., 2016. Poly(ester amide)s: Recent insights into synthesis, stability and biomedical applications. Polym. Chem. 7, 7039.
Wojnarowska, Z., Paluch, M., 2016. Tautomerism in drug delivery. In: Descamps, M. (Ed.), Disordered Pharmaceutical Materials. Wiley-VCH Verlag GmbH & Co.. Chapter 7.
Wübbenhorst, M., van Turnhout, J., 2002. Analysis of complex dielectric spectra I. One-dimensional derivative techniques and three-dimensional modelling. J. Non Cryst. Solids 305, 40–49.
Yang, C., Su, X., Liu, A., Zhang, L., Yu, A., Xi, Y., Zhai, G., 2013. Advances in clinical study of curcumin. Curr. Pharm. Des. 19, 1966–1973.
Yousefzade, O., Valenti, S., Puiggali, J., Garmabi, H., Macovez, R., 2019. Segmental relaxation and partial crystallization of chain-extended poly(L-Lactic Acid) reinforced with carboxylated carbon nanotube. J. Polym. Sci Part B: Polym. Phys. 57, 222–233.
Zachariah, M., Romanini, M., Tripathi, P., Barrio, M., Tamarit, J.L., Macovez, R., 2015. Self-diffusion, phase behavior, and Li+ ion conduction in succinonitrile-based plastic Co-crystals. J. Phys. Chem. C 119, 27298–27306.
Zhou, D., Zhang, G., Law, D., Grant, D., Schmitt, E., 2002. Physical stability of amorphous pharmaceuticals: Importance of configurational thermodynamic quantities and molecular mobility. J. Pharm. Sci. 91, 1863–1872.